NUMERICAL STUDY OF THE TEKKEN WELDING TEST

A. A. M. PAGET*,**, V. ROBIN**,****, J. DRAUP***, S. HENDILI**, R. UFARTÉ**, T. KHAN*,***, J. DELMAS**, M. C. SMITH*

**The University of Manchester (MaSC), M13 9PL, Manchester, United-Kingdom*
***EDF R&D (PRISME), 78401, Chatou, France*
****EDF Energy R&D UK Center (MaSC), M13 9PL, Manchester, United-Kingdom*
*****EDF Direction Technique, 69007, Lyon, France*

Corresponding Author ORCiD: 0000-0002-3090-2414

DOI 10.3217/978-3-85125-968-1-25

ABSTRACT

To improve the assessment methods of the cold cracking risk, the usage of the Tekken welding test is proposed. The test load is generated by the residual stresses, whose magnitude is controlled by the size of the Tekken mock-up. In order to conduct a subsequent test benchmarking campaign, the optimum dimensions providing a suitable, realistic load are sought. A 2D computational model is developed to answer this question. A range of thicknesses from 15 mm to 150 mm is investigated. An enrichment by experimental data allows predictions with a great level of confidence. For the welding parameters and metals selected, it is found that the level evolution of the self-restraint conditions reaches a stabilization above a thickness of 50 mm. Moreover, the non-negligible effect of the solid-solid phase transformation induced material property changes is highlighted.

Keywords: cold cracking, residual stresses, Tekken test, metallic microstructure, nuclear industry

INTRODUCTION

GENERAL BACKGROUND

As one of the world's major electricity operators and with 73 operating reactors on several continents, the *EDF group* faces some technical challenges in maintaining and modernizing its fleet of nuclear power plants. The research presented here is motivated by the need to qualify innovative repair methods and accredit them with the local regulatory bodies. More precisely, we are focusing on repair methods using nickel-based alloys for ferritic steel components of the nuclear steam supply system, the core element of a pressurized water reactor.

Part of the technical solution explored here is focused on cladding using multi-pass welding, optimized with bead tempering principles [1]–[6] in place of additional

conventional heatings to tackle their difficulties of execution. Indeed, these additional heating steps are generally applied [7] for such massive parts to meet a high level of quality and safety of the welding bead deposition during the manufacturing processes [8], as well as for repair operations only if the component can be accessible or disassembled and manipulated. However, in contrast with the oil & gas industry, most of the elements constituting a nuclear reactor cannot be easily accessible or removed, because of reduced space, structural embedment, and radioactivity (often from the component itself).

Therefore, to address the necessity to increase the expertise on these innovative methods prior to their deployment in the nuclear industry, several experimental and numerical analyses are being conducted. Among others, the base metal resistance to cold cracking [8] must be assessed in the weld configuration proposed for these new methods (this is also known as *hydrogen assisted cold cracking*, *delayed cracking*, or *under-bead cracking* [9]). To conduct this assessment, strong couplings between experiments and modelling are of great interest to inform and/or validate each other. Within this research project [10], one of the objectives is to establish a comparative benchmark between a conventional welding quality test and another, potentially more realistic test, respectively the implant and Tekken tests [5], [11]–[15]. Both are allowed by the standard *ISO 17642* for characterizing the risk of cold cracking. This comparison allows the following to be assessed:

- First, the performance of the Tekken test in comparison with the implant test. The latter is historically used in France for welding process qualification of potentially susceptible components.
- Second, the accuracy of further computational models able to quantify the margins against cold cracking.

All the modelling presented here was undertaken using the platform *Salome_Meca* [16]. The finite element solver used was *Code_Aster* [17]. Both are open-source software and code developed by *EDF* with other partners.

TEKKEN TEST: LITERATURE REVIEW

The Tekken test was conceived and developed by the *Technical Research Institute of the Japanese National Railways* [11]. This is a self-restraint test made from a plane-slotted specimen, as shown in Fig. 1. High stress state is achieved by the slot/slit and groove characteristics and the mock-up thickness [14], [18], [19]. It was principally designed for quantitatively assessing base metal weldability in a configuration representative of the intended application thanks to its massiveness and intrinsic architecture. The Tekken test focuses mainly on assessing the risk of cold cracking. It can be also used for other defect types within the base and/or the weld metal. It requires good repeatability in the case of non-cracking to confirm this result. The Tekken specimen has been studied by a number of researchers who have provided relevant conclusions on the slot/slit types, shapes, and locations within this monolithic mock-up [20]–[23]. However, it is still difficult to estimate or even to find in the literature accurate details of the stress state surrounding the weld of a Tekken test.

METHOD APPROACH

Based on previous research, it was decided to conduct this research project [10] with centered y-slit Tekken and circular V-notched implant designs.

In parallel, prior to manufacture the Tekken specimens, it was decided to conduct a series of computational studies to optimize the specimen thickness. The local stress level increase with thickness, at the expense of higher material consumption. It was decided to aim at maximum load in order to generate the highest risk of cold cracking.

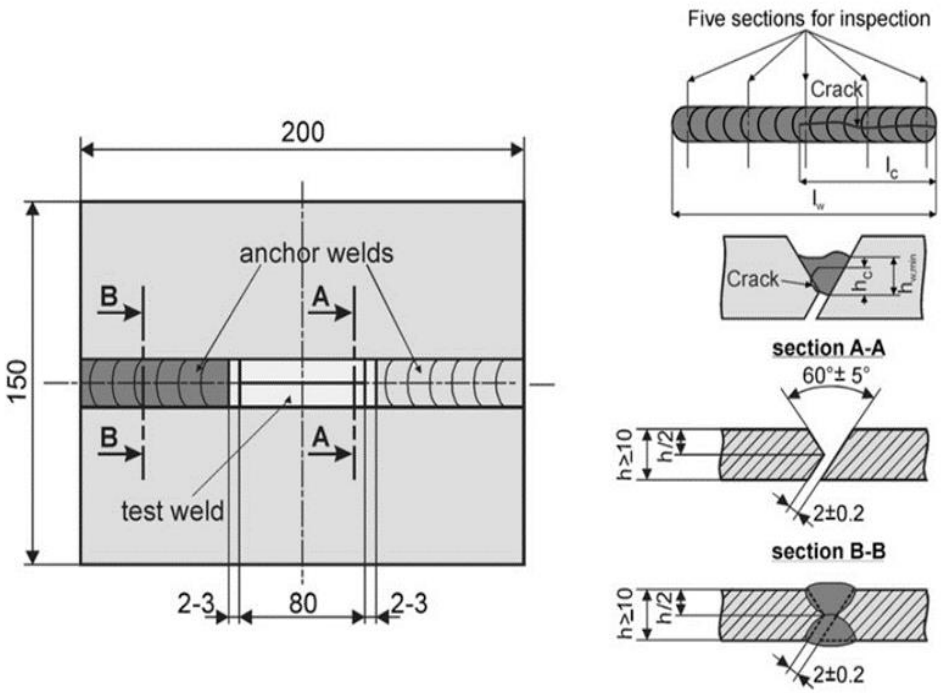

GLOBAL VIEW CROSS-SECTIONAL VIEWS

Fig. 1 Illustration of a Tekken test mock-up ; before & after the weld bead deposition [11]

A 2D thermo-metallo-mechanical finite element model was constructed to compare the evolution of local stress level depending on the mock-up thickness. The 2D idealization ensures a good ratio between the calculation duration and sufficient accuracy of the results. The model represents a mid-length transverse cross-section of a Tekken mock-up, as shown in Fig. 2. This ignores the perturbations at the welding start and stop regions at the bead extremities. Models were generated and run for a full range of different mock-up thickness (15 mm to 150 mm), allowing rapid identification of the stress state level for each Tekken size, for the base and filler metals selected and for welding parameters previously defined by parallel experiments.

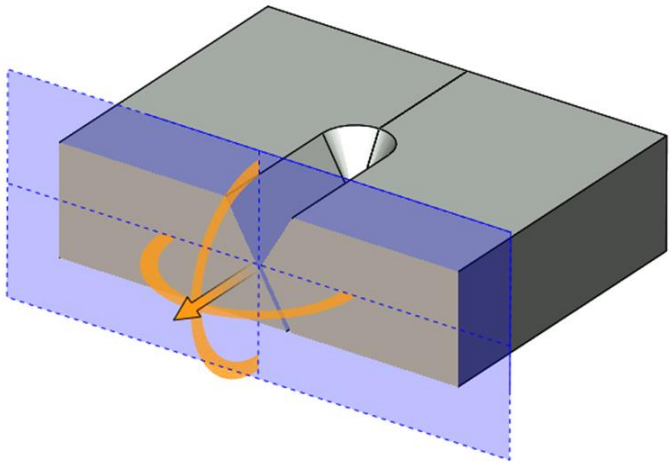

Fig. 2 Illustration of the modelled 2D slice position within the Tekken test mock-up

MATERIAL DATA

The base metal employed is from a *18MND5* material batch whose chemical composition diverges slightly from specification, allowing it to be treated – *only for research purposes* – as a *16MND5*, commonly used for manufacturing reactor pressure vessels. It is equivalent to similar specifications such as *SA-508 Grade 3 Class 1* or *SFVV3* [24], [25]. The filler metal utilized is nickel-based alloy *52M*, which has been selected previously for the proposed repair procedure. A potential application is repairs to the nickel-based alloy *182* welds which join the vessel to the bottom-mounted instrumentation nozzles. The exact metal chemical compositions are given in Table 1, as well as additional details.

The thermal, metallurgical and mechanical properties used in the simulations have been principally identified by several previous studies carried out by *EDF* with different partners [26]. These have been supplemented with updated values from recent studies. In order to reliably reproduce the actual mechanical properties of this metal batch after quenching-tempering-rolling operations, the initial distribution of micro-constituents was assumed to be a mixture made of 61 % ferrite and 39 % bainite (which may not reflect the real microstructure composition).

In addition, some major features considered in all the simulations presented in this study can be highlighted. For the base metal:

- Metallo-dependent elasto-visco-plastic model, including the effects of the solid-solid phase transformation induced plasticity and of the strain-hardening recovery
- Grain growth modelling during the austenitization steps (driving parameter for the micro-constituent fraction predictions)

Concerning the filler metal:

- Chaboche elasto-visco-plastic model (parameters recently calibrated within parallel studies [27], [28])

Table 1 Chemical composition analysis of the employed metal batches (values from the material certificates provided by the suppliers *Creusot-Loire Industries* and *Special Metals Corporation*)

Base Metal											
considered designation	**C**	**Si**	**Mn**	**Ni**	**Cr**	**Mo**	**P**	**S**	**Cu**	**V**	**Al**
16MND5 *rolled quenched tempered*	0,181	0,216	1,53	0,625	0,202	0,479	0,0063	0,0029	0,111	≤ 0,005	0,022
Filler Metal											
commercial designation	**C**	**Si**	**Mn**	**Ni**	**Cr**	**Mo**	**P**	**S**	**Cu**	**Co**	**Al**
Inconel 52M (coiled wire)	0,017	0,12	0,72	59,36	30,05	0,01	0,004	0,001	0,03	0,006	0,11
	Nb + Ta	**Fe**	**Al + Ti**	**Ti**	**B**	**Zr**	**other**				
	0,83	8,49	0,34	0,23	0,001	≤ 0,01	≤ 0,50				

In order to refine the microstructure prediction abilities used for the particular chemical composition of this steel batch, a specific continuous cooling transformation diagram was calculated using a tool recently developed at the *Modelling and Simulation Center (EDF & The University of Manchester)*, based on Li's model [29]–[32]. However, a preliminary estimation of the austenitization temperature and prior austenite grain size range that could be typically encountered in the gas tungsten arc-welding process was necessary. Considering the observations of [29], a range from 3 µm to 130 µm was adopted. Hence, the average value (66 µm) and the commonly considered temperature of welding molten pools (1 450 °C [33], [34]) were utilized to run this continuous cooling transformation diagram calculation. It was directly returned under a table format readable by the *Code_Aster* solver. An overview of this continuous cooling transformation diagram is given in Fig. 3. During simulation, the feature enabling this solver to adapt its interpretation of the continuous cooling transformation diagram as function of the calculated grain size was activated.

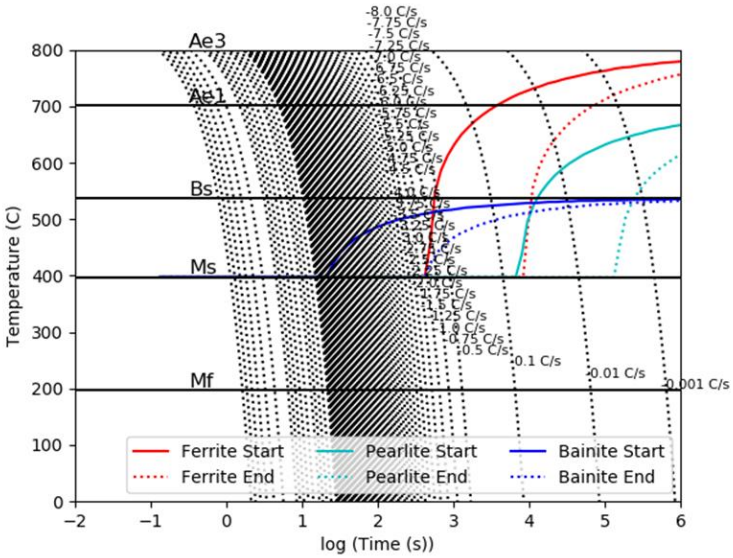

Fig. 3 Representation of the continuous cooling transformation diagram calculated for the base metal (each dotted line represents a cooling rate step)

SIMULATION: FIRST CALIBRATION & QUALIFICATION

DILATOMETRY

Different thermal cycles have been explored using dilatometry testing in parallel studies [27], [28], [35]. In a few words, a dilatometry machine measures the material expansion as a function of the temperature. It allows investigation at the same time of both conventional thermal expansion behavior and solid-solid phase transformation. The experimental data produced on the base metal have been used as reference to assess the reliability of the numerical continuous cooling transformation data set utilized in the welding simulation. Testing has been performed both on the used *16MND5* material lot, and also on the *SA-508 Grade 3 Class 1* steel. The 2D axisymmetric modelling of the dilatometry test specimen (half-rod) comprised an imposed heating temperature (reproducing the induction heating), a heat exchange (reproducing the convective loss and gas cooling), and the radiation loss. The nodes of one half-rod end were considered as embedded along the longitudinal direction, and the nodes of the half-rod axis of symmetry as fixed along the transverse direction. The displacement was therefore followed using the nodes on the other half-rod end. The mesh was built of 125 linear quadratic elements about 400 µm × 400 µm.

A few examples of the predicted temperature-strain cycles compared with the experiments are presented in Fig. 4 & 5. Agreement is generally good, confirming the suitability of the calculated continuous cooling behavior.

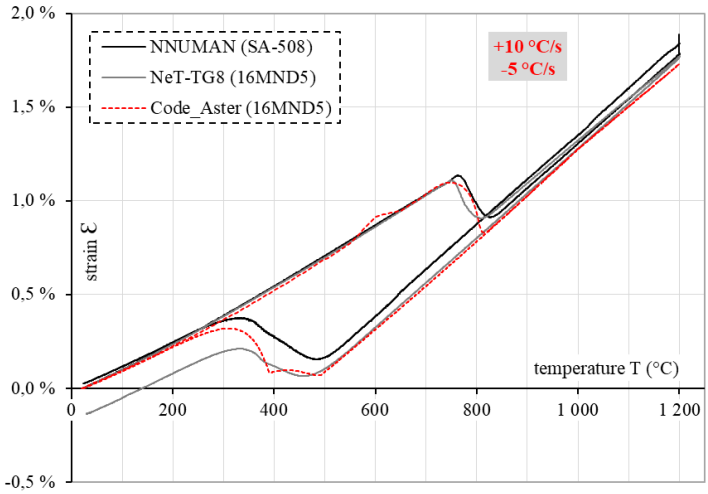

Fig. 4 Comparison between the simulated *16MND5* behavior and the experimental observations for this modelled steel (*NeT–TG8* project [27], [28]) as well as for the *SA-508* (*NNUMAN* project [35], [36])

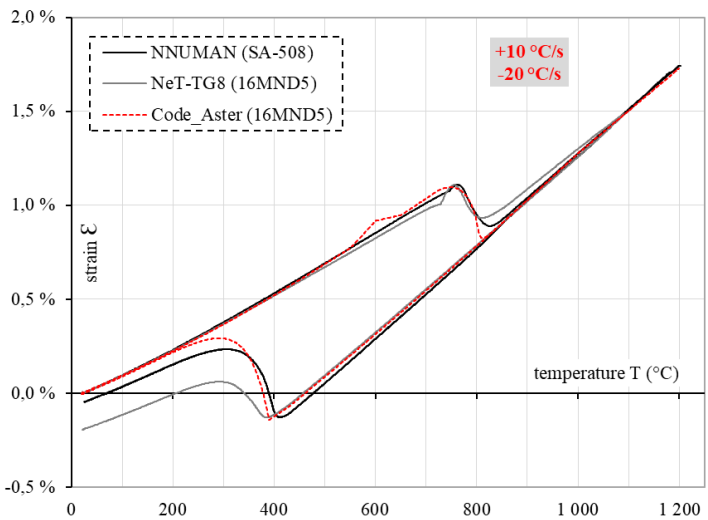

Fig. 5 Comparison between the simulated *16MND5* behavior and the experimental observations for this modelled steel (*NeT–TG8* project [27], [28]) as well as for the *SA-508* (*NNUMAN* project [35], [36])

TEKKEN MODELLING

MESHING STRATEGY

As presented above in Fig. 2, only slices representing the mid-length transverse cross-section of the Tekken mock-ups were modelled in 2D. The meshes were built of linear quadratic elements (4 977 for the 30 mm specimen). Particular attention was paid to the element refinement and quality in the critical areas surrounding the weld bead. The element size adopted in these locations is about 250 µm, and it is gradually increased in the remote areas that were expected to be relatively unaffected. The weld bead thickness was estimated of 4,5 mm.

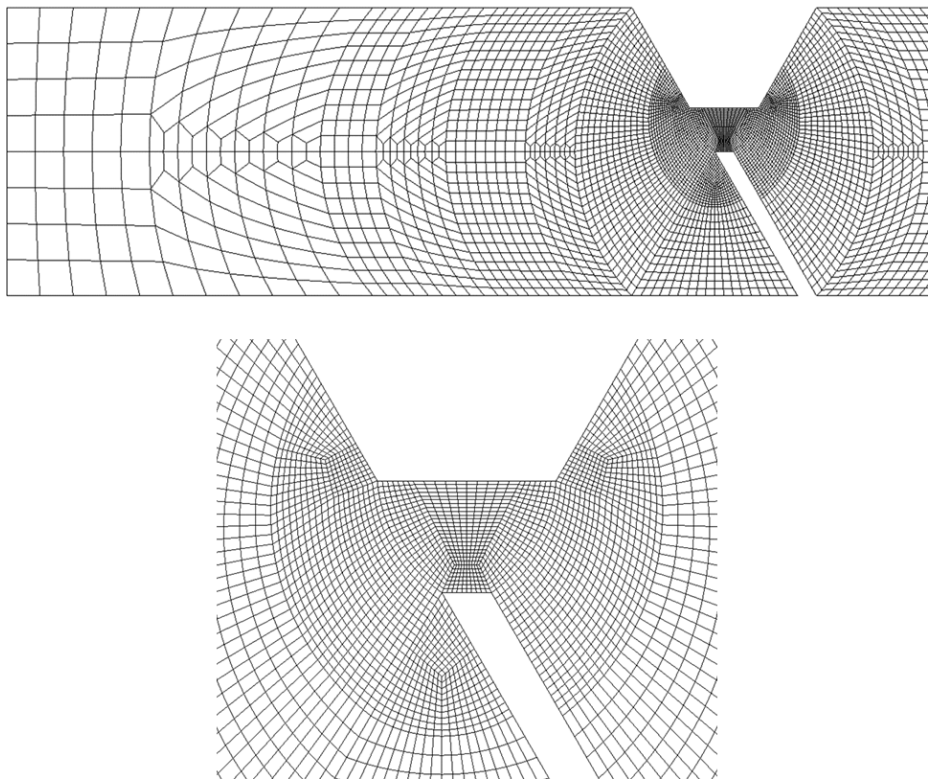

Fig. 6 Illustrations of the mesh generated for a mock-up thickness of 30 mm

The sketching and meshing operations were fully executed using *Python* command script instructions for *Salome_Meca*. To aid computation, the slices were sub-divided into different zones constituting the global geometry and then concatenated. Some illustrations of the mesh modelling the 30 mm thick mock-up are given in Fig. 6.

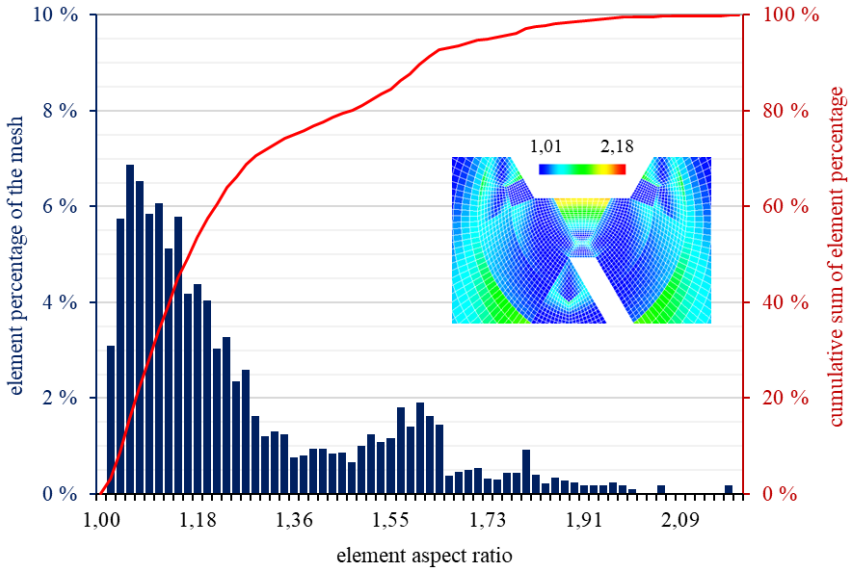

Fig. 7 Results of the mesh element quality control, the criterion being based on the shape ratio of the quadrangles (size: 30 mm thick)

The global element quality assessment has shown that 82 % of the elements have an aspect ratio inferior at 1,5 , which is considered acceptable for this study (refer to Fig. 7). In particular, elements within the heat-affected zone and fusion zone all have relatively good aspect ratios despite of the geometry singularities. The method utilized for calculating this ratio is given with Equations (1)-(2)-(3) [16]. Note that a perfect square would have a ratio equal to 1,0.

$$q = \frac{L_{max}(L_0+L_1+L_2+L_3)}{4A} \qquad A = \frac{1}{2}\left\|\overrightarrow{L_0} \times \overrightarrow{L_1}\right\| + \frac{1}{2}\left\|\overrightarrow{L_3} \times \overrightarrow{L_2}\right\| \qquad (1)\ (2)$$

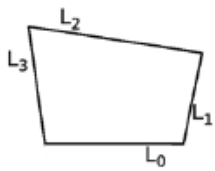

$$L_{max} = \max(L_0, L_1, L_2, L_3) \qquad (3)$$

AUTOMATION OF COHERENT MESHING'S

Considering the wide range of Tekken mock-up thicknesses to investigate, a sampling of representative thicknesses was selected: every 5 mm from 15 mm to 50 mm thick, then every 10 mm from 50 mm to 100 mm, and a final thickness of 150 mm. This resulted in a total of 14 Tekken tests to simulate.

The meshing command script was coded to automatically adjust the element sizes when necessary to ensure suitable junctions at the refinement zone frontiers. The element size of the critical area mentioned previously was however imposed. In addition, the biggest element size (at the mock-up edges) was set at 3 mm for mock-ups under 25 mm thick, and then at 4 mm for other sizes.

This algorithmic automation has permitted the Tekken test meshes to be produced with constant and coherent characteristics, to minimize the risk of mesh differences confusing the results. Fig. 8 illustrates this with the extreme cases, 15 mm and 150 mm thick.

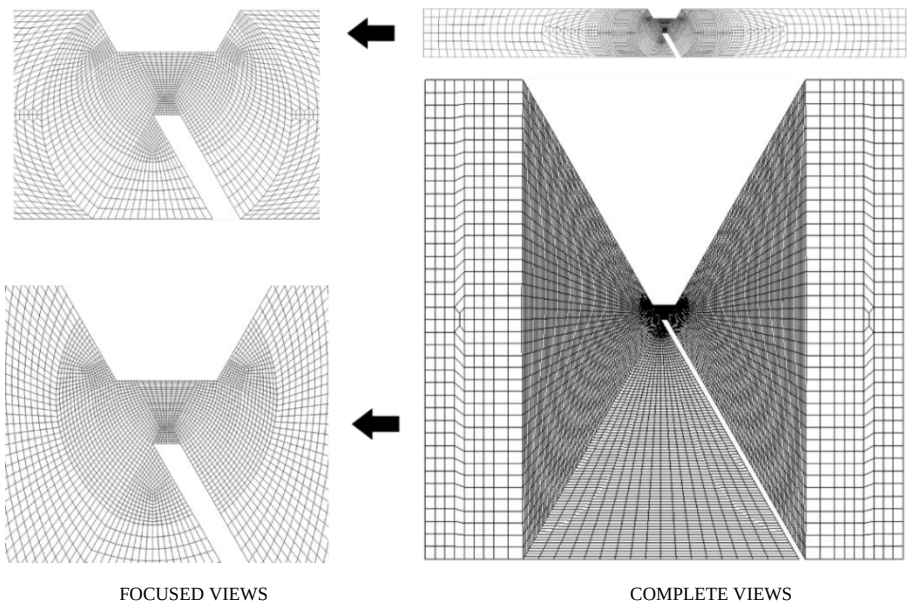

Fig. 8 Coherence illustration from the 15 mm to the 150 mm meshes with a focus on the weld bead area

BOUNDARY CONDITIONS

Conventional convection exchange and radiation loss were taken into account in the thermal calculation. The value of the convection exchange with air was set at $h = 15\ \mathrm{W{\cdot}m^{-2}{\cdot}K^{-1}}$, which is slightly superior to a natural convection in order to add the effect of the shielding gas flow. The emissivity coefficient was assumed at $\mathcal{E} = 0{,}50$ as the average value for ground or machined steel surfaces. In the mechanical calculation the nodes of the two slice extremities were considered as fully embedded for reproducing the mock-up stiffness (refer to Fig. 9).

MODELLING OPTIMIZATION

The selected modelling type was axisymmetric about the Y-axis. This approach allows more realistic out-of-plane constraint than mathematical plane strain, and aids mechanical solution convergence in *Code_Aster*, according to the developer team.

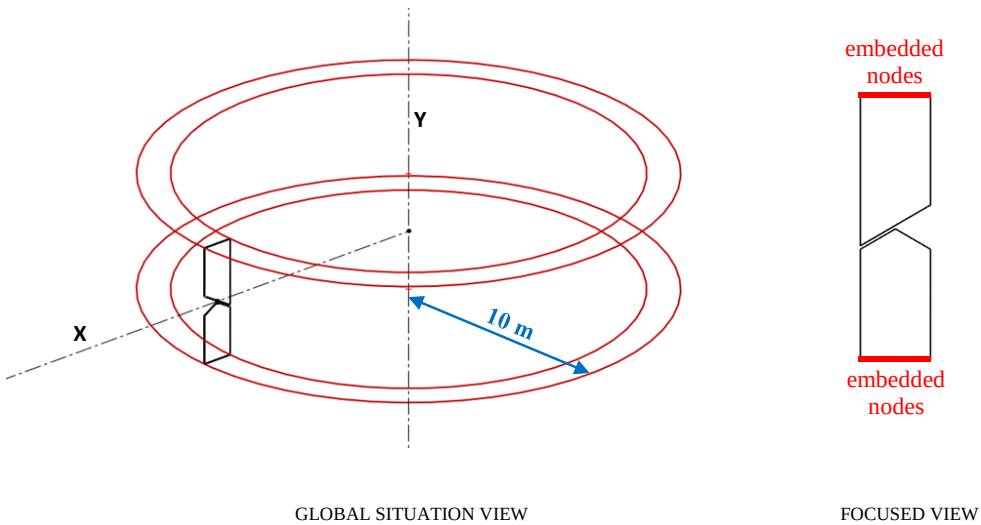

Fig. 9 Schematic view of the mesh re-positioning (modified scale) and mechanical boundary conditions

However, the Tekken test specimens are not axisymmetric. Therefore, the modelled mock-up has been rotated by 90°, and placed at 10 meters from the Y-axis to give an effectively infinite radius and tackle the non-axisymmetry of this test device. The impact of this large radius was successfully examined by a quick comparison with one meter shorter and one meter longer radii: the results were not affected. Fig. 9 summarizes this re-positioning.

EQUIVALENT HEAT SOURCE

The heat input induced by the electric arc was reproduced through an imposed time-depended heat flux H_{flux} on the weld metal elements. This was simply composed of two stages: a heating phase as described in Equations (4) and a cooling phase as described in Equations (5).

$$H_{flux} = \frac{Q_{max}}{Dt_1 \times t} \qquad (4)$$

$$H_{flux} = \frac{Q_{max}}{Dt_2 \times (t - (Dt_1 + Dt_2))} \qquad (5)$$

Fig. 10 The thermocouple-instrumented mock-up before assembly and after the welding run completion

For calibrating the parameters of this modelled heat source, a thermocouple-instrumented Tekken test was performed at *EDF* with the welding parameters selected for this research project [10]. These have been optimized within parallel studies [27], [28], [37] to ensure the weld bead deposition quality, as well as maximizing the hydrogen absorption (deliberate placement in unfavorable conditions [38]–[40]). These welding parameters are detailed in Table 2.

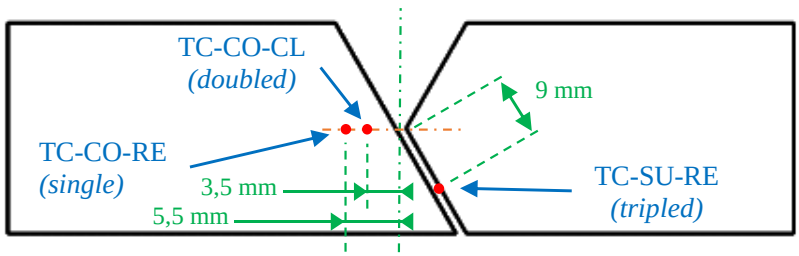

Fig. 11 Thermocouple locations utilized for the heat source calibration with a 40 mm Tekken mock-up

Welds were deposited using a robotized tungsten inert gas welding station *Valk Welding VWPR QE Extern* (composed of a *VWPR-TIG I* welding torch and a *WGIII-E1400* robot system (*Panasonic TA-1400* model)). A 40 mm thick mock-up made from two parts was utilized (Figure 10). *K*-type thermocouples were placed at five different buried and surface locations. The device utilized for recording the temperatures is a *NI 9213 / cDAQ 9174* acquisition system supplied by *National Instruments*, coupled with the software *LabVIEW – SignalExpress*. The Tekken test device was then placed on special supports designed to minimize the heat transfer to the welding table. Some thermocouple locations were doubled or tripled to determine repeatability. For this study calibration, only three positions were selected in order to get rid of any potential perturbations caused by the heat source shape assumptions. They are detailed in Fig. 11.

Table 2 Welding parameters selected for this research project

parameter	value
shielding gas	*Linde – Varigon 5* (5 % H_2 + 95 % Ar)
gas flow rate	11,0 ± 0,3 l/min
welding torch travel speed	0,12 m/min
nominal current intensity	240 ± 1 A
pulsing frequency	0 Hz (direct current)
filler wire feeding speed	3,0 m/min
contact-tip to workpiece distance	30,75 ± 0,50 mm
standoff distance	21,25 ± 0,35 mm
electrode stick out	15,00 ± 0,1 mm
electrode extension	24,50 ± 0,25 mm
arc length (from groove bottom)	6,25 ± 0,25 mm
filler metal wire-electrode distance	2,50 ± 0,25 mm
gas cup internal diameter	Ø 11,25 ± 0,10 mm
filler metal wire diameter	Ø 0,9 mm
arc polarity	electrode [-]
electrode	tungsten – 2 % lanthanum
electrode diameter	Ø 2,4 mm
electrode angle	30°
arc voltage control feature (A.V.C.)	enabled
voltage	15,60 ± 0,75 V
welding process type	tungsten inert gas (T.I.G.)
deposited metal section	15,9 mm²
linear energy	18,7 kJ/cm
average power	3,7 kW

Following the welding test, the three thermal cycle curves from the experiment were generated by first synchronizing the time axis, and then averaging when doubled or tripled. A wide range of heat source parameter combinations were simulated using a

design of experiment matrix. Then, the set providing the most suitable match in terms of peak temperatures and cooling rates was selected. Hence, the identified parameters used in Equations (4)-(5) was Q_{max} = 18,0 J, Dt_1 = 6,0 s and Dt_2 = 8,6 s. The heating phase has been considered as having a limited effect for this study needs. The base material heat capacity function has been also slightly adjusted. The comparison between the experimental data and the obtained simulation results with the calibrated heat source are presented in Fig. 12.

Although there is a certain degree of uncertainty about how suitable this calibration would be for other mock-up thicknesses, which still have slight meshing differences, these parameters were assumed as being constant.

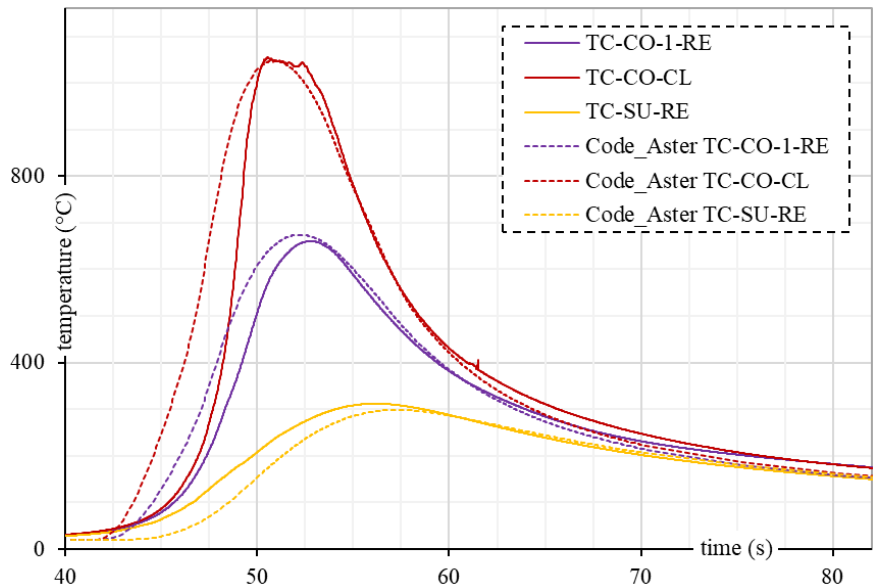

Fig. 12 Comparison of the experimental thermocouples data with the virtual ones of the *Code_Aster* simulation after the heat source parameter calibration using a 40 mm Tekken test mock-up

RESULTS

Once the thermal model was calibrated, the 2D thermo-metallo-mechanical simulation was run on each mesh. According to [41], mainly a uniform normal stress is experienced by bead deposited in an oblique y-slot. Considering this, the temporal evolution of the nodal loads on the restrained faces (as shown in Fig. 9) was extracted and used to estimate the average normal stress σ_{avg} occurring on the weld bead cross-section. This last value was then utilized as the benchmark criterion for studying the effect of thickness. This comparison is presented in Fig. 13 at a focused time scale. Fig. 14 shows an observation over a period of 10 hours for the 15 mm, 30 mm and 50 mm specimens.

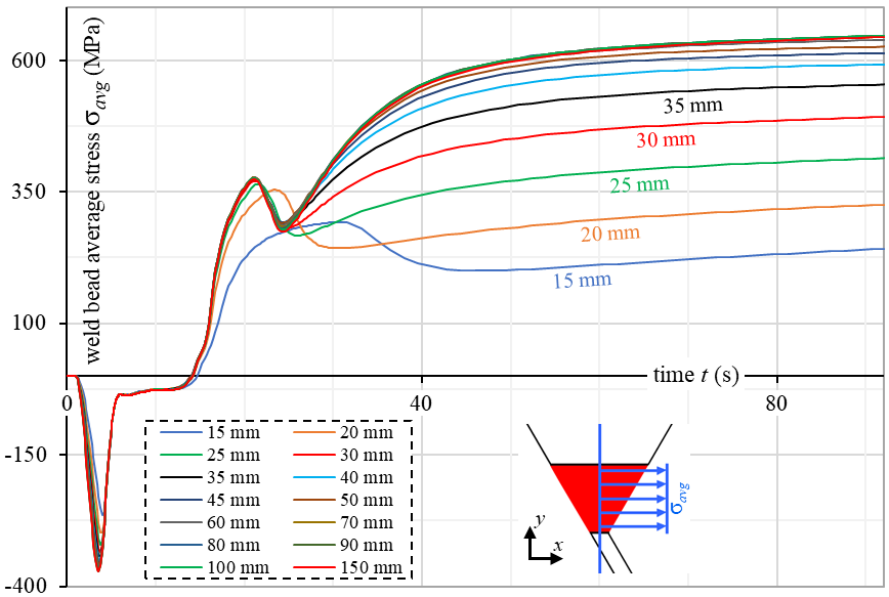

Fig. 13 Benchmarking of the relative effect of the Tekken mock-up thickness on the average stress σ_{avg} experienced by the weld bead perpendicular cross-section (relative stress value)

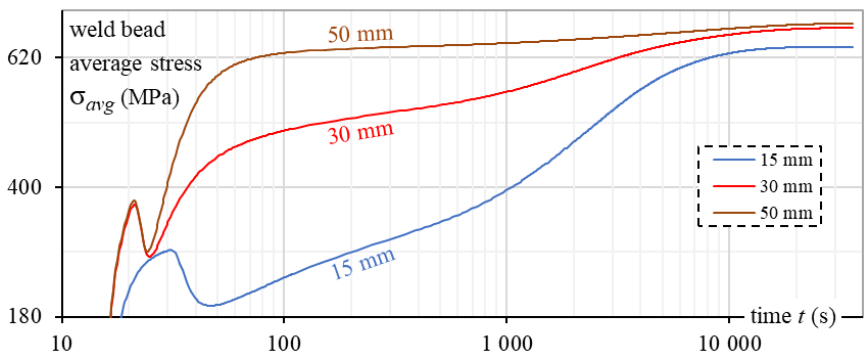

Fig. 14 Average stress σ_{avg} evolution 10 hours after the weld completion for the 15 mm, 30 mm and 50 mm Tekken specimens (relative stress value)

DISCUSSION

The results show a compressive stress state during the filler metal deposition and the beginning of the cooling. This is in line with the experimental observations by indirect measurement conducted by [21] using similar y-slit crack test specimens. However, this must be treated with caution : the simulation approach considers the weld metal elements already in place before their simulated deposition (no “inactive element method”), without a deactivation or mitigating feature for their thermo-mechanical characteristics (no “quiet element method”). Considering that the weld metal is molten at this stage, the magnitude of this first part of the mechanical results cannot be considered as entirely correct. Only the results after complete metal solidification can be exploited here. According to the experimental and computational results produced, it can be estimated that the weld metal is fully solidified approximately five seconds after the passage of the welding torch. At that stage, the stress state is more or less equal to zero.

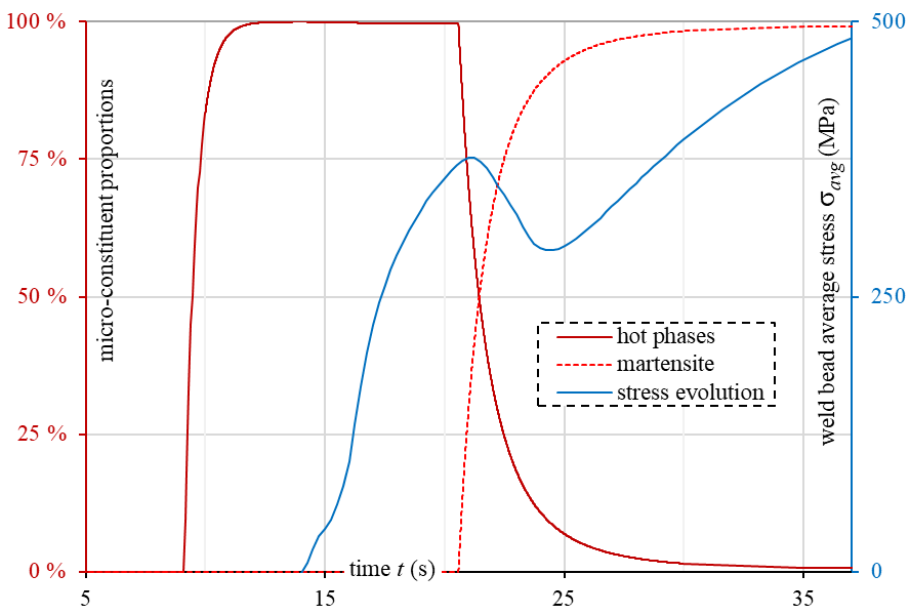

Fig. 15 Focus on the thermocouple *TC-CO-CL* location (Tekken 40 mm) : correlation between the drop in the stress increase during the metallurgical changes

Following this, rapid growth of the tensile stress is observed, until a sudden drop. The divergences for the smallest thicknesses start at the end of this first stress increase. The drop observed results from metallurgical changes (solid-solid phase transformations), principally from “hot” to “cold” micro-constituents, as seen previously with the dilatometry testing. This aspect has been studied in detail by [42], who measured a similar drop in magnitude during their welding test. This is mainly caused by the atomic re-arrangement occurring within the unit cells during solid-solid transformations, as well as differences in the thermo-mechanical properties of the different micro-constituents. This

correlation is shown in Figure 15 with a 40 mm Tekken mock-up by focusing on the local changes surrounding the closest thermocouple to the fusion boundary (*TC-CO-CL*).

After solid-solid phase transformations are complete, the tensile stress increase resumes. The increasing rate is rather moderated in the thinnest specimen thicknesses due to their lower mass, which reduces the cooling rate. From this point onwards, there is a net effect of the thickness. The maximum achievable self-restraint condition is reached above a thickness of 50 mm. It can take more than 10 hours to experience the final residual stress level. Moreover, it was found that this stabilization phenomenon is insensitive to variations of the material and equivalent heat source parameters made during the model calibration steps, which raised confidence in these findings.

CONCLUSION

A numerical study enriched by experimental analyses was conducted to develop understanding of the Tekken welding test. The finite element model was used to investigate the effect of mock-up thickness on the self-restraint conditions. The thickness is often considered as the major parameter for driving the stress state self-generated in this test device [14], [18], [19], [43].

Nevertheless, there was a lack of precise information on this impact. This study has permitted to propose a qualitative estimation through a first approach in 2D. A complete benchmarking of the different thicknesses was established, focusing on the level of the average normal stress experienced by the weld bead. The following are the main findings:

- Although the standard Tekken design allows thicknesses up to 150 mm, the residual stress saturates above a thickness of 50 mm using these materials and welding parameters.
- Moreover, this saturation stress is rapidly reached at such thicknesses because of fast heat dissipation into the material remote from the weld. This demonstrates that the mechanical loading peaks quickly after weld completion when the hydrogen level is at its peak, which is thereby the moment when the risk of cold cracking occurrence is the highest.

Thanks to this study and the established benchmarking, it has been possible to conclude that for the remainder of this research project [10], a thickness approaching 50 mm would provide the best compromise for quickly maximising the stress state using this metal combination with these specific welding parameters.

RECOMENDATIONS

Finally, this study has also permitted to identify several elements that would require further development :

- Quantitively speaking, the convergence to a maximum stress state of about 650 MPa may seem plausible (relative value). Nevertheless, this would require additional verifications before any conclusion on the absolute values of the residual stress experienced. For instance, an extensive experimental small-scale testing under different temperature intervals and for several microstructure types of this base metal would be of interest to finely adjust its material properties and calibrate the model.
- Improvements of the meshing strategy are now possible using the weld macrography realised at the end of this project. This would allow modelling of the actual weld bead shape, the y-slot dimensions, fusion boundaries, and heat-affected zone limits.
- The equivalent heat source could also be improved by modelling its shape accurately and refining its parameters using the experimentally measured isotherm boundaries.
- The calculation duration could be optimised by applying simpler material behaviour models to regions outside the heat-affected zone.
- Prior austenite grain size is an important variable, as the prediction of the micro-constituent proportions within the heat-affected zone is highly dependent on this parameter. This only had an impact in the smallest thicknesses, since heat dissipation there was insufficient to lead to fully martensitic heat-affected zones. However, a lack of experimental data and model development makes optimisation of this part of the solver difficult.
- Finally, a transposition to a 3D model would be of interest to validate a part of the assumptions made for these 2D simulations.

ACKNOWLEDGEMENTS

We warmly thank the researchers and technicians who were involved in the dilatometry test projects (*NeT–TG8* and *NNUMAN* programs [27], [28], [35], [36]) for having kindly shared their experimental results.

We also very appreciated the help and the quality of the work undertaken by the staff from all the different entities across England and France, from the specimen manufacture to their analyses, as well as for the computational model developments.

Bibliographic References

[1] P. BRZIAK, M. ŁOMOZIK, R. MIZUNO and F. MATSUDA: 'Repair Welding of SQV2A Pressure Vessel Steel by Temper Bead Techniques Without Post Welding Heat Treatment', *Archives of Metallurgy and Materials*, vol. 56, no. 2, Jan. 2011, Document identifier = DOI: 10.2478/v10172-011-0024-x.

[2] V. ROBIN and P. GILLES: 'Prevention des risques d'apparition de defaut par la simulation numerique des procedes de fabrication', in *10ème colloque national en calcul des structures*, Giens, France, 2011, Document URL: https://hal.archives-ouvertes.fr/hal-00592704 (consulted on 03/10/2019).

[3] A. S. ALORAIER, A. AL-MAZROUEE, J. W. H. PRICE and T. SHEHATA: 'Weld repair practices without post weld heat treatment for ferritic alloys and their consequences on residual stresses: A review', *International Journal of Pressure Vessels and Piping*, vol. 87, no. 4, pp. 127-133, Apr. 2010, Document identifier = DOI: 10.1016/j.ijpvp.2010.02.001.

[4] A. S. ALORAIER, R. N. IBRAHIM and J. GHOJEL: 'Eliminating post-weld heat treatment in repair welding by temper bead technique: role bead sequence in metallurgical changes', *Journal of Materials Processing Technology*, vol. 153-154, pp. 392-400, Nov. 2004, Document identifier = DOI: 10.1016/j.jmatprotec.2004.04.383.

[5] M. CONSONNI: 'A review of the machine GTAW ambient temperature temper bead repair technique for nuclear power plant components', *Members Technical Literature Review - TWI Ltd (The Welding Institute)*, 2013, Document identifier = TWI ref.: 22952.

[6] J.-M. CARPREAU, S. FABRICE, C. GILLES and D. BASTIEN: 'Soudage Temperbead applique aux materiaux nucleaire', presented at the *Journées Nationales du Soudage 8 - Matériaux*, EDF R&D Chatou, 2010.

[7] G. K. PADHY, V. RAMASUBBU, N. MURUGESAN, C. REMASH and S. K. ALBERT: 'Effect of preheat and post-heating on diffusible hydrogen content of welds', *Science and Technology of Welding and Joining*, vol. 17, no. 5, pp. 408-413, Jul. 2012, Document identifier = DOI: 10.1179/1362171812Y.0000000023.

[8] J.-M. CARPREAU: 'Fissuration et soudage', presented at the *EDF (Électricité De France)*, 8éme Colloque Modélisation et simulation Numérique du soudage, 2010.

[9] G. K. PADHY and Y. KOMIZO: 'Diffusible hydrogen in steel weldments: a status review', *Transactions of JWRI (Joining and Welding Research Institute of Osaka University)*, vol. 42, no. 1, pp. 39-62, Jun. 2013, Document identifier = ISSN: 03874508.

[10] A. A. M. PAGET: *Exploration of the cold cracking risks and limits for welding repair applications of low-alloy ferritic steel nuclear components*, PhD thesis, University of Manchester, Manchester, 2023.

[11] T. KANNENGIESSER and T. BOELLINGHAUS: 'Cold cracking tests – an overview of present technologies and applications', *Weld World*, vol. 57, no. 1, pp. 3-37, Feb. 2013, Document identifier = DOI: 10.1007/s40194-012-0001-7.

[12] S. DEBIEZ and P. GERARD: 'Pratique et signification de l'essai de fissuration a froid sur implant', *Soudage et Techniques Connexes*, 1980.

[13] S. DEBIEZ: 'Determination des conditions de soudage des aciers faiblement allies pour prevenir le risque de fissuration a froid', *Soudage et Techniques Connexes*, vol. 38, no. 5, pp. 188-205, 1984.

[14] H. GRANJON: 'Informations sur les essais de fissuration', *Soudage et Techniques Connexes*, pp. 7-8, 1963.

[15] A. TALEBI HANZAEI, S. P. H. MARASHI and E. RANJBARNODEH: 'The effect of hydrogen content and welding conditions on the hydrogen induced cracking of the API X70 steel weld', *International Journal of Hydrogen Energy*, vol. 43, no. 19, pp. 9399-9407, May 2018, Document identifier = DOI: 10.1016/j.ijhydene.2018.03.216.

[16] SALOME_MECA: *EDF (Électricité de France) & CEA (Commissariat à l'Énergie Atomique et aux Énergies Alternatives)*, Document URL: www.salome-platform.org.
[17] CODE_ASTER: *EDF (Électricité de France)*, Document URL: www.code-aster.org.
[18] R. KURJI and N. CONIGLIO: 'Towards Establishment of Weldability Test Standards for Hydrogen Assisted Cold Cracking', *International Journal of Advanced Manufacturing Technology*, vol. 77, pp. 1581-1597, 2015, Document identifier = DOI: 10.1007/s00170-014-6555-3.
[19] W. CAMPBELL: 'Experiences with HAZ cold cracking tests on a C-Mn structural steel', *Welding Journal*, vol. 55, no. 5, 1976.
[20] K. SATOH and T. TERASAKI: 'Effect of joint geometry on stress concentration factor at the root of weld', *Journal of the JWS (Japan Welding Society)*, vol. 48, no. 5, pp. 298-303, 1979, Document identifier = DOI: 10.2207/qjjws1943.48.298.
[21] F. MATSUDA, H. NAKAGAWA, K. SHINOZAKI and H. KIHARA: 'Evaluation of transformation expansion and its beneficial effect on cold crack susceptibility using Y-slit crack test instrumend with strain gauge', *Transactions of JWRI (Joining and Welding Research Institute of Osaka University)*, vol. 13, no. 1, pp. 47-55, Jul. 1984, Document identifier = DOI: 10.18910/6144.
[22] R. D. STOUT, R. VASUDEVAN and A. W. PENSE: 'A field weldability test for pipeline steels', *Welding Journal - Welding Research Supplement*, vol. 55, no. 4, pp. 89s-94s, Apr. 1976, Document URL: http://files.aws.org/wj/supplement/WJ_1976_04_s89.pdf.
[23] R. VASUDEVAN, R. D. STOUT and A. W. PENSE: 'A field weldability test for pipeline steels – part II', *Welding Journal - Welding Research Supplement*, vol. 59, no. 3, pp. 76s-84s, Mar. 1980, Document URL: http://files.aws.org/wj/supplement/WJ_1980_03_s76.pdf.
[24] L. M. DAVIES: 'A comparison of Western and Eastern nuclear reactor pressure vessel steels', *International Journal of Pressure Vessels and Piping*, vol. 76, no. 3, pp. 163-208, Mar. 1999, Document identifier = DOI: 10.1016/S0308-0161(97)00075-6.
[25] M. YU, Y. J. CHAO and Z. LUO: 'An assessment of mechanical properties of A508-3 steel used in chinese nuclear reactor pressure vessels', *J. Pressure Vessel Technol*, vol. 137, no. 3, pp. 031402-031402–7, Jun. 2015, Document identifier = DOI: 10.1115/1.4029434.
[26] V. CANO and J. ANGLES: 'Recueil bibliographique de caractéristiques thermiques, métallurgiques et mécaniques de l'acier 16MND5', *EDF (Électricité De France)*, EDF R&D Clamart, EDF internal publication H-T64-2008-03224-FR, Mar. 2010.
[27] X. S. QINGRONG: 'NeT TG8 - dissimilar metal welding between 18MnD5 and alloy 52 - final technical report', *EDF - UoM – MaSC*, University of Manchester, Post-Doctoral technical report, Jun. 2019.
[28] V. ROBIN ET AL.: 'Net Project Task Group 8 – an international benchmark on residual stress assessment for welding repair', presented at the *PVP2022 - ASME 2022 Pressure Vessels and Piping Conference*, Las Vegas, Nevada, 2022, vol. Volume 4B: Materials and Fabrication, Document identifier = DOI: 10.1115/PVP2022-85083.
[29] Y. L. SUN ET AL.: 'Effects of dilution on alloy content and microstructure in multi-pass steel welds', *Journal of Materials Processing Technology*, vol. 265, pp. 71-86, Mar. 2019, Document identifier = DOI: 10.1016/j.jmatprotec.2018.09.037.
[30] M. V. LI, D. V. NIEBUHR, L. L. MEEKISHO and D. G. ATTERIDGE: 'A computational model for the prediction of steel hardenability', *Metall Mater Trans B*, vol. 29, no. 3, pp. 661-672, Jun. 1998, Document identifier = DOI: 10.1007/s11663-998-0101-3.
[31] C. J. HAMELIN ET AL.: 'Validation of a numerical model used to predict phase distribution and residual stress in ferritic steel weldments', *Acta Materialia*, vol. 75, pp. 1-19, Aug. 2014, Document identifier = DOI: 10.1016/j.actamat.2014.04.045.
[32] J. DRAUP: 'Python based Continuous-Cooling-Transformation (CCT) digitizer tool', *EDF Energy R&D (UK Center - MaSC)*, University of Manchester, EDF internal publication UKC-R-2018-0xx (provisional), Dec. 2019.

[33] J. ANGLES: 'Modélisation et Simulation de la Fissuration à Froid: Etude numérique d'une maquette pour la préparation d'essais', *EDF (Électricité De France)*, EDF R&D A.M.A., EDF internal publication H-T59-2011-02090-FR, 2011.

[34] M. SOKOLOV, A. SALMINEN, E. I. KHLUSOVA, M. M. PRONIN, M. GOLUBEVA and M. KUZNETSOV: 'Testing of new materials and computer aided optimization of laser beam welding of high-strength steels', *Physics Procedia*, vol. 78, pp. 255-264, Jan. 2015, Document identifier = DOI: 10.1016/j.phpro.2015.11.036.

[35] M. C. SMITH, A. N. VASILEIOU, D. W. RATHOD, J. FRANCIS, N. M. IRVINE and Y. SUN: 'A review of welding research within the new nuclear manufacturing (NNUMAN) programme', presented at the *PVP2017 - ASME 2017 Pressure Vessels and Piping Conference*, Waikoloa, Hawaii, 2017, vol. Volume 6B: Materials and Fabrication, Document identifier = DOI: 10.1115/PVP2017-66180.

[36] G. OBASI ET AL.: 'Measurement and prediction of phase transformation kinetics in a nuclear steel during rapid thermal cycles', *Metall and Mat Trans A*, vol. 50, no. 4, pp. 1715-1731, Apr. 2019, Document identifier = DOI: 10.1007/s11661-018-05102-y.

[37] A. FERRARI: 'Dosages d'hydrogène réalisés avec le procédé TIG automatique et l'emploi d'un fil Inconel 52M sur substrat en acier faiblement allié 18MnNiMo5', *IS groupe (Institut de Soudure)*, IS technical report 4325-5G465Y-V1, Feb. 2021, Document identifier = IS ref.: 4325-5G465Y-V1.

[38] A. OUDRISS ET AL.: 'Consequence of the diffusive hydrogen contents on tensile properties of martensitic steel during the desorption at room temperature', *Materials Science and Engineering: A*, vol. 598, pp. 420-428, Mar. 2014, Document identifier = DOI: 10.1016/j.msea.2014.01.039.

[39] V. ROBIN: 'Chapter 1 - Industrial challenges where computational welding mechanics becomes an engineering tool', in *Thermomechanical industrial processes*, J.-M. Bergheau, Ed. *ISTE Ltd & John Wiley & Sons*, 2013, pp. 1-74, Document identifier = ISBN: 978-1-84821-358-6.

[40] V. ROBIN, F. GOMMEZ, C. PRIMAULT and J. DEVAUX: 'Implant test modeling for risk of cold cracking assessment during welding operations', presented at the *PVP2012 - ASME 2012 Pressure Vessels and Piping Conference*, Toronto, 2012, pp. 557-565, Document identifier = DOI: 10.1115/PVP2012-78376.

[41] N. YURIOKA and H. SUZUKI: 'Hydrogen assisted cracking in C-Mn and low alloy steel weldments', *International Materials Reviews*, vol. 35, no. 1, pp. 217-249, Jan. 1990, Document identifier = DOI: 10.1179/imr.1990.35.1.217.

[42] F. MATSUDA, H. NAKAGAWA, K. SHINOZAKI, Y. NISHIO and H. KIHARA: 'Effect of transformation expansion on restraint stress of weldment in relation to cold cracking of high strength steels', *Transactions of JWRI (Joining and Welding Research Institute of Osaka University)*, vol. 11, no. 2, pp. 57-65, Dec. 1982, Document identifier = DOI: 10.18910/9554.

[43] A. L. WINGROVE: *An appraisal of the Tekken test*, PhD thesis, University of Wollongong, Wollongong, 1986, Document URL: https://ro.uow.edu.au/cgi/viewcontent.cgi?referer=https://scholar.google.com/&httpsredir=1&article=2606&context=theses (consulted on 05/10/2021).